Received: 28 January 2022 | Revised: 29 March 2022 | Accepted: 11 April 2022

DOI: 10.1002/nano.202200027

RESEARCH ARTICLE

nano select Open Access WILEY

Multi-parametric surface plasmon resonance-based intake quantification of label-free light-activated nanoparticles by therapeutic limbal stem cells for corneal blindness

Maija Kauppila[1] | **Roosa Ståhlberg**[1] | **Vitor Francisco**[2] | **Lino Ferreira**[2,3] | **Heli Skottman**[1]

[1]Faculty of Medicine and Health Technology, Tampere University, Tampere, Finland

[2]CNC - Centro de Neurociências e Biologia Celular, CIBB - Centro de Inovação em Biomedicina e Biotecnologia, University of Coimbra, Coimbra, Portugal

[3]Faculty of Medicine, University of Coimbra, Coimbra, Portugal

Correspondence
Heli Skottman, Faculty of Medicine and Health Technology, Tampere University, Arvo Ylpön katu 34, 33520 Tampere, Finland.
Email: heli.skottman@tuni.fi

Abstract

Advanced therapies with combined approaches of cell and nanomedicine-based interventions are emerging. Corneal blindness with a severe form of limbal stem cell (LSC) deficiency is an example of defect with unmet clinical need. Towards cell-based therapy, advanced enabling technologies are needed for efficient intracellular delivery of biomolecules both for in vitro disease modeling and for in vivo interventions. For this nanomedicine creates novel possibilities as light activatable polymeric nanoparticles (NPs) hold potential for controlled on-demand cargo delivery with control of light. In this study, we used multi-parametric surface plasmon resonance (MP-SPR) technique in vitro for measuring NP intake in real-time by therapeutic LSCs. Although a variety of NPs has been described, many challenges remain, and one is related to cell uptake of the formulations. Here, three different NP formulations were analyzed, one demonstrating clearly the highest cellular intake by LSCs. Importantly, data demonstrate that the labeling of NPs significantly reduce the cellular intake highlighting the importance of label-free administration and quantification. The MP-SPR based approach hold high potential as a powerful non-invasive platform to be implemented in manufacturing of therapeutic cell- and cargo-based interventions. For any therapy applications, validated non-invasive and label independent NP intake measurement systems would be important.

KEYWORDS
cornea, human pluripotent stem cells, intake, label-free, limbal stem cells, nanoparticle

1 | INTRODUCTION

Advanced clinical therapies with combined approaches of cell- and nanomedicine-based interventions are emerging, and ophthalmic applications are in the front row due to the easy access of the eye and cutting-edge imaging and surgical technologies already available. Corneal blindness is a serious problem worldwide accounting for ~2 million new cases annually and adding a huge burden to families and health care resources.[1] Often, the

This is an open access article under the terms of the Creative Commons Attribution License, which permits use, distribution and reproduction in any medium, provided the original work is properly cited.
© 2022 The Authors. *Nano Select* published by Wiley-VCH GmbH.

26884011, 2022, 8, Downloaded from https://onlinelibrary.wiley.com/doi/10.1002/nano.202200027 by Tampere University Foundation, Wiley Online Library on [10/01/2023]. See the Terms and Conditions (https://onlinelibrary.wiley.com/terms-and-conditions) on Wiley Online Library for rules of use; OA articles are governed by the applicable Creative Commons License

only treatment is corneal transplantation limited by shortage of donor tissue. Moreover, significant loss or dysfunction of limbal stem cells (LSCs) can result in LSC deficiency (LSCD), which is difficult to treat as cadaveric donor corneas do not contain living LSCs.[2] There are many causes of LSCD including hereditary aniridia-related keratopathy and acute trauma, for example, chemical burns. LSCD is characterized by disruption of cornea epithelium renewal and loss of the limbus barrier, leading to the invasion of conjunctiva, inflammation, loss of corneal clarity, and in severe cases blindness.[2,3] The only viable long-term treatment strategy would enable the re-establishment of LSC reservoir in the limbus via rejuvenation of remaining LSCs (e.g., biomolecule-based interventions for partial LSCD) or regenerative homing of new transplanted LSCs. Towards that end, advanced enabling technologies are needed for efficient intracellular delivery of therapeutic biomolecules (i.e., antisense oligonucleotides and siRNAs) both for in vitro disease modeling and drug targeting approaches, as well as for on-demand in vivo interventions. For this nanomedicine creates novel possibilities as polymeric nanoparticles (NPs) hold potential for controlled cargo delivery.[4–6] As an example, technology could be applied in vitro for modifications of LSCs before transplantation to patient's eye and targeted cargo release could be induced in vivo based on the personalized clinical need of a patient.

The possibilities enabled by light activatable polymeric NPs is especially appealing for corneal applications with targeted on-demand cargo released with control of light. Compared with other external triggers, light offers clear advantages, including: (i) precise control of the size of the area being irradiated by varying the beam of the laser, providing a higher level of spatial control; and (ii) the possibility of having a system that responds to different wavelengths for multiple drug release.[7] The major advantage of external light stimulus is being a non-invasive method and light-responsive NPs have been successfully used in ophthalmic drug delivery systems in vitro and in vivo.[8–11]

Although a variety of NPs has been described, many challenges remain to be addressed and one is related to the efficient cellular uptake of the formulations. Importantly, non-invasive tools to validate the NP intake by the therapeutic cells are needed. Common intake validation methods include confocal microscopy, transmission emission microscope, flow-cytometry and inductively coupled plasma mass spectroscopy (ICP-MS).[12–15] These methods are mostly end-point techniques, and they require fixation of cells, and most of them require additional labeling of samples with fluorescent labeled molecules. For any therapy applications, validated non-invasive and label independent NP intake measurement systems implemented to the good manufacturing practice (GMP) cell production would be important. For that, multi-parametric surface plasmon resonance (MP-SPR) technique measuring NP intake in real-time and in a label-free manner could be an ideal option in future.

The aim of this study was to quantify the intracellular intake rate of near visible light activatable polymeric NP to find out which NP formulation would be the most prominent delivery tool for therapeutic applications using LSCs. Additionally, real-time label-free intake measurement method was compared to previously used imaging-based technique, which is possible to carry out only with labeled NPs and fixed cells. Given the high level of interest in NP based carriers, it was surprising to realize that there are, to our knowledge, no reports describing methods for studying the real-time intake of label-free NP by LSCs and especially with LSCs differentiated from human pluripotent stem cells (hPSC-LSCs) providing novel and highly scalable source of LSCs for regenerative applications.[16–18]

2 | RESULTS AND DISCUSSION

2.1 | Light-activated NPs

2.1.1 | Light-activated NP production and characterizations

To evaluate MP-SPR technique in cellular NP intake, we selected three different NP formulations, C11, P1C5, and P1C7, that already show high accumulation and important cytoplasmic release in different cell types due to their different physico-chemical properties.[19–21] The characterization of the NPs by dynamic light scattering (DLS) showed a mean particles size of 123.4 ± 11.3, 348.1 ± 32.4, and 184.4 ± 10.5 nm for C11, P1C5, and P1C7, respectively. Furthermore, the zeta potential measurements showed positive charged NPs, 14.8 ± 3.5, 24.8 ± 3.1, and 24.6 ± 2.4 mV for C11, P1C5, and P1C7, respectively. For the preparation of the NPs, we used polymers with photocleavable linkers, which upon light activation allow the release of their cargo, such as non-coding RNAs. After irradiation of P1C5 or P1C7 NPs with near visible UV-A light (365 nm) used in this study or alternatively with blue light (405 nm), occurs the generation of nitrosobenzene group due to cleavage of the photo-cleavable ester bond in the polymers forming the NPs, leading to NPs disassembly. On the other hand, C11 NPs are disassembled upon changes in the hydrophobic-hydrophilic balance due to cleavage of the DMNC light sensitive group incorporated in the NPs. In order to label the NPs, we covalently attached fluorescein isothiocyanate (FITC) to the amine groups of the NPs. The DLS measurements of the NPs showed similar size and zeta potential values between the unlabeled and FITC-labeled NPs and the difference in NPs diameter between unlabeled and FITC labeled NPs are within standard

26884011, 2022, 8, Downloaded from https://onlinelibrary.wiley.com/doi/10.1002/nano.202200027 by Tampere University Foundation, Wiley Online Library on [10/01/2023]. See the Terms and Conditions (https://onlinelibrary.wiley.com/terms-and-conditions) on Wiley Online Library for rules of use; OA articles are governed by the applicable Creative Commons License

deviation (Table S1 and S2). The disassembly of NPs can be also rapidly monitored by DLS, even when the NPs are unlabeled with a dye (Table S1). However, for conventional cellular intake studies either NPs or cargo must be labeled to monitor internalization by cells. The stability overtime of unlabeled and FITC labeled NPs suspended in CnT-30 cell culture medium was confirmed with DLS (Figure S1).

2.1.2 | Light toxicity measurements for the hPSC-LSCs

One of the challenges of light-triggerable NPs is related to the potential deleterious effects of light stimuli, which can arise from the direct interaction between light and the tissues or indirectly via the photoactivation mechanism of nanoformulations. In previous studies by others, it has been demonstrated that when ultraviolet light B (UV-B)-irradiation (0.02 J cm^{-2}) is used for primary human LSCs it caused significant reduction of LSC proliferation and loss of LSC characteristics, as putative stem cell marker expression is significantly decreased.[22] Thus, UV irradiation can damage LSCs, but the possible damage depends both on the wavelength and power density used. In our study, we use lower time of exposure (10 minutes) and higher wavelength (365 nm) UV-A irradiation which translates into lower power density (1.0 mW cm^{-2}). To validate biocompatibility of the light activated NPs with therapeutic and highly sensitive hPSC-LSC in vitro, the UV light toxicity assay was conducted with 365 nm UV-A light used in this study. Based on the cellular morphology and growth, 10-minute UV irradiation did not affect hPSC-LSC viability, and this is supported by the high cell viability in LIVE/DEAD® viability assay (Figure S2A, B). Additionally, UV-irradiated hPSC-LSCs expressed the same well-acknowledged LSC marker proteins (ΔNp63α detected with double staining of p63/p40 and CK14) as non-irradiated control hPSC-LSCs (Figure S2C) which further support the conclusion that UV irradiation has at least no visible toxic effects on hPSC-LSC. Importantly, the safety and any possible side effects of the UV-A light needs to be determined very carefully in vivo before any consideration for the possible clinical use in future.

2.2 | MP-SPR live cell assay establishment for targeted cell types

2.2.1 | MP-SPR method establishment with HeLa cells

The MP-SPR live cell assay method has been previously used with HeLa cells.[23] Thus the method establishment in our study for hPSC-LSCs was first conducted with HeLa cells as well (Figure S3, S5). Further, Akl and co-workers have recently reported live cell NP intake with MP-SPR using HT-29 cells.[24] Both of these previous studies used different cell types, different NPs and excluded comparative analyses of labeled and unlabeled NPs. Nevertheless, these studies provide proof-of-concept that the MP-SPR technology could be applicable also with more sensitive therapeutic hPSC-LSCs. Based on the first experiments with HeLa cells, the MP-SPR method was slightly adapted by introducing NP samples through sample loops for 14 minutes and measuring 30 minutes post-injection. Data analysis was adjusted subtracting 785 nm signal from 670 nm (peak minimum angle) to reduce background signal and cell number on sensor slides that may occur even when having 100% confluent sensor slides.

2.2.2 | MP-SPR live cell assay establishment and au sensor slide coating optimization for hPSC-LSCs

First, Au sensor slide coating was optimized to promote hPSC-LSC adhesion in clinically applicable serum-free condition previously established[25] and to reach relevant stemness maintaining cell confluency and morphology characteristics for hPSC-LSC on Au sensor slide. Based on the optimization phase, 5 μg mL^{-1} collagen V (CIV) + 0.5 μg mL^{-1} laminin 521 (L521) coating was chosen for the MP-SPR experiments as hPSC-LSCs were successfully cultured and grown over Au sensor slides with this coating method (Figure 1). In each experiment, the Au sensor slide confluency was validated before and after MP-SPR measurement and representative images of hPSC-LSCs on sensor slides are shown in Figure S4.

2.2.3 | Validation of MP-SPR measurement set-up for hPSC-LSC

Next, stable measurement conditions for MP-SPR was established with hPSC-LSCs. The Figure 2 presents the full SPR curve of the hPSC-LSCs over the sensor slide compared to the blank Au sensor. With cells on the sensor slide, the peak minimum angle differs 3° to 4° from blank Au sensor slide since the mass is increased over the sensor slide. In addition, the Total Internal Reflection (TIR) angle becomes rounder which is a typical phenomenon for thick and heterogenous layers on top of a sensor slide such as cells. Measurement accuracy is confirmed by having peak minimum to remain sharp on the SPR curve as the signal-to-noise ratio is of better quality with sharp TIR. Before starting NP injections, the hPSC-LSC stability over

26884011, 2022, 8, Downloaded from https://onlinelibrary.wiley.com/doi/10.1002/nano.20220027 by Tampere University Foundation, Wiley Online Library on [10/01/2023]. See the Terms and Conditions (https://onlinelibrary.wiley.com/terms-and-conditions) on Wiley Online Library for rules of use; OA articles are governed by the applicable Creative Commons License

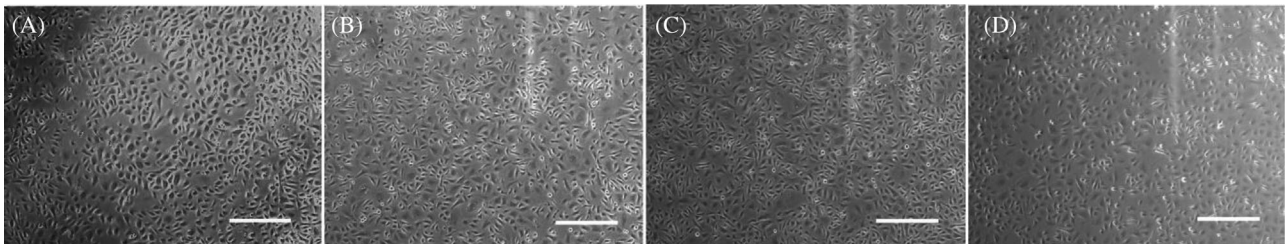

FIGURE 1 hPSC-LSCs culture optimization over coated SPR Au sensor in comparison to plastic chamber slide. (A) hPSC-LSC morphology on 4-well Chamber Slide with 5 μg cm^{-2} CIV + 0.5 μg cm^{-2} L521 (control). The hPSC-LSC morphology on SPR Au sensor with (B) 5 μg cm^{-2} CIV + 0.5 μg cm^{-2} L521 coating, (C) 10 μg cm^{-2} CIV + 1.0 μg cm^{-2} L521 coating, and (D) with 4.5 μg cm^{-2} fibronectin. Different coatings on Au sensors (n = 2 for each coating) had no visible effect on cell morphology and thus, standard cell culture coating was selected for further analyses in this study. Scale bar is 500 μm

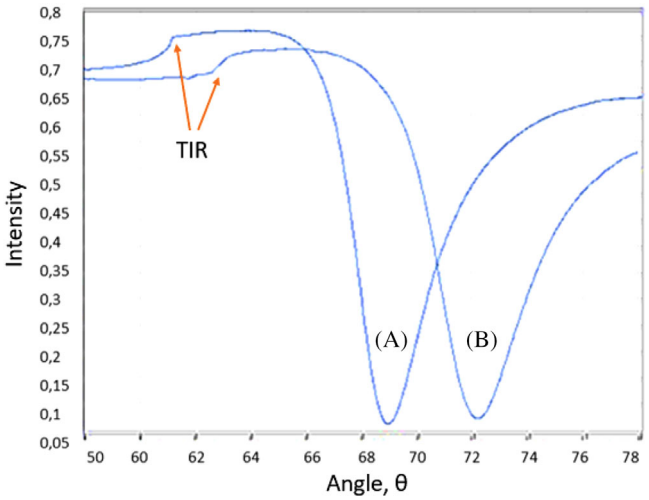

FIGURE 2 Representative SPR curve comparison between blank Au sensor slide and hPSC-LSCs grown on sensor slide. Curve A presents the blank Au sensor SPR curve and curve B the SPR curve of confluent hPSC-LSC monolayer over Au sensor slide. The peak minimum angle has shifted 3–4° and remained sharp and TIR has become a bit rounder. Each hPSC-LSC sample (n = 19) was measured before introduction of NPs

surface is validated by measuring that a stable baseline can be achieved.

2.2.4 | hPSC-LSC NP intake results with MP-SPR

The intake of the three NP formulations C11, P1C7, and P1C5 by hPSC-LSC was first analyzed with MP-SPR using both FITC labeled and label-free NPs (Figure 3). Due to different chemical composition of the NPs, different amounts of FITC could be covalently attached to the formulation and may influence cell intake. However, the NP characterization results shows similar attachment of FITC in the three NPs, 9.6 ± 0.1, 9.8 ± 0.1, and 9.5 ± 0.1 μg per mg of NP for C11, P1C5, and P1C7, respectively.

The MP-SPR method can be implemented for the confluent cell monolayer grown on the SPR gold sensor surface coated with extracellular matrix proteins, which is stimulated with the NPs, while simultaneously measuring the complete SPR angular spectra as a function of time. The increase of the SPR signal indicates cellular changes in the basal side of cells caused by the NP uptake in the apical side of the cell. An increase of NP uptake increases also cellular reorganization and after the NP injection is stopped, the remaining responses indicate the level of cellular response that remains after the flow of NPs is ended. Importantly, MP-SPR measurement method is highly sensitive and measurement accuracy depends on multiple factors: the cell culture media flow in reference channel or the NP-culture media suspension in measurement channel should not contain any air bubbles. In addition, cells on the sensor slide should remain attached and the flow-rate should be consistent. Also, the measurement accuracy can be affected if cells are not forming a confluent monolayer over the sensor slide. All these parameters were monitored during the experimentations.

As a result, the label-free P1C7 signal (mDeg) recorded with MP-SPR was higher with 50 μg mL^{-1} (except one 50 μg mL^{-1} sample without response) (Figure 3E) than with 20 μg mL^{-1} sample concentration (Figure 3B) and the signal was lower when FITC-labeled P1C7 was injected (Figure 3H), with 8 mDeg difference between maximum average signal of 50 μg mL^{-1} label-free and labeled NPs (Table S4). Similarly, label-free P1C5 intake signal (mDeg) was higher with 50 μg mL^{-1} sample concentration (except one 50 μg mL^{-1} sample without response) (Figure 3F) than with 20 μg mL^{-1} (Figure 3C) and the intake signal was lower when NPs were FITC-labeled (Figure 3I), with 7 mDeg difference between maximum average signal of 50 μg mL^{-1} label-free and labeled NPs (Table S4). Of the note, one of the 20 μg mL^{-1} P1C5 sample caused a high peak in the beginning of injection and then decreases to

26884011, 2022, 8, Downloaded from https://onlinelibrary.wiley.com/doi/10.1002/nano.202200027 by Tampere University Foundation, Wiley Online Library on [10/01/2023]. See the Terms and Conditions (https://onlinelibrary.wiley.com/terms-and-conditions) on Wiley Online Library for rules of use; OA articles are governed by the applicable Creative Commons License

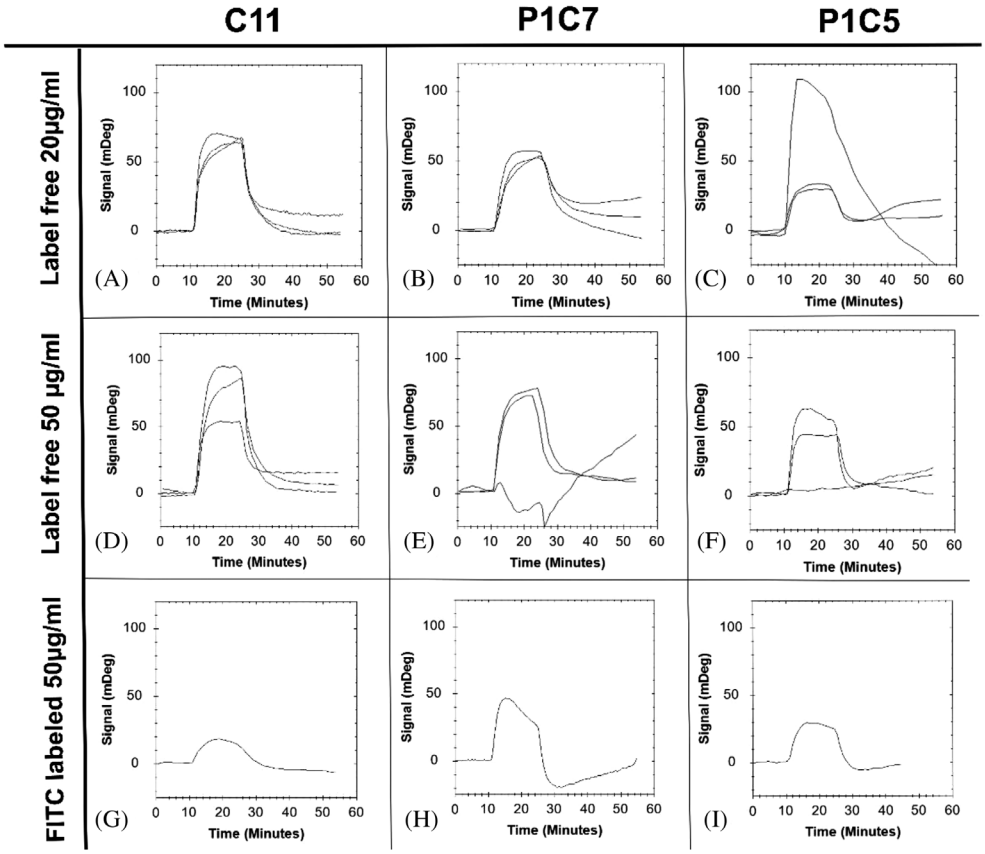

FIGURE 3 The intake of the three NP formulations C11, P1C7, and P1C5 by hPSC-LSC analyzed with MP-SPR using both label-free and FITC-labeled NPs. (A) label-free 20 μg mL^{-1} C11 (n = 3), (B) label-free 20 μg mL^{-1} P1C7 (n = 3), (C) label-free 20 μg mL^{-1} P1C5 (n = 3), (D) label-free 50 μg mL^{-1} C11 (n = 3), (E) label-free 50 μg mL^{-1} P1C7 (n = 3), (F) label-free 50 μg mL^{-1} P1C5 (n = 3), (G) FITC labeled 50 μg mL^{-1} C11 (n = 1), (H) FITC labeled 50 μg mL^{-1} P1C7 (n = 1), and (I) FITC labeled 50 μg mL^{-1} P1C5 (n = 1)

negative signal. This could be caused by aggregated NPs binding over the sensor surface spot which does not contain cell, or there can be noise signal from the reference channel caused by air bubble. The decrease of the signal supports the view that P1C5 NPs did not cause cellular reorganization and uptake. Among the three NP formulations in use, the NP formulation C11 gave the highest NP intake signal (mDeg) and again, the signal was greater with 50 μg mL^{-1} (Figure 3D) than with 20 μg mL^{-1} sample concentration (Figure 3A) demonstrating a clear concentration dependent intake rate. With this NP formulation as well, the signal was significantly lower when FITC-labeled C11 was injected (Figure 3G) and the difference between maximum average signal of 50 μg mL^{-1} unlabeled and labeled NPs was 60 mDeg (Table S4). Thus, all three label-free NP formulations showed concentration dependency with MP-SPR sensorgrams and the C11 and P1C7 NPs did not show saturation in their intake curves. P1C5 on the other hand, had very flat injection profile, once maximal signal was reached excluding one 20 μg mL^{-1} sample where measurement accuracy can be argued. Overall, the smallest NP particle C11 gave more consistent measurements between biological replicates (higher variation with P1C7 and P1C5 NPs) which may be related to most efficient and consistent uptake. Interestingly, NP labelling with FITC was clearly reducing the intake of all three NP formulations. In addition, NP intake rate correlates with the NP size: highest signal was recorded with smallest C11 and lowest with largest P1C5 NP formulation. The maximum signal of hPSC-LSCs recorded during the NP injection are shown in Table S4 further demonstrating this trend.

2.2.5 | hPSC-LSC NP intake validation with confocal microscopy

To validate NP intake further by hPSC-LSC, the confocal imaging was performed with FITC-labelled NPs (Figure 4). As a result, the intake of all three NP formulations was confirmed but due to the limited intake efficacy of all three labeled NPs, there was no clear NP formulation or concentration dependent difference between 20 and 50 μg mL^{-1}

26884011, 2022, 8, Downloaded from https://onlinelibrary.wiley.com/doi/10.1002/nano.202200027 by Tampere University Foundation, Wiley Online Library on [10/01/2023]. See the Terms and Conditions (https://onlinelibrary.wiley.com/terms-and-conditions) on Wiley Online Library for rules of use; OA articles are governed by the applicable Creative Commons License

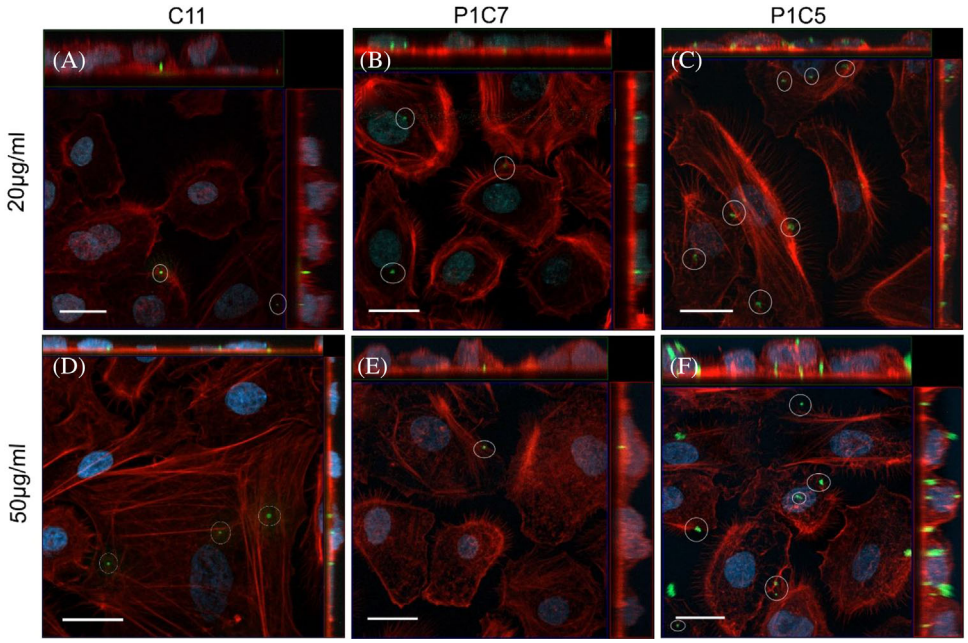

FIGURE 4 The intake of the FITC labeled NP formulations C11, P1C7 and P1C5 by hPSC-LSC analyzed with confocal microscopy. (A–C) 20 µg mL^{-1} FITC labeled NP intake, (D–F) 50 µg mL^{-1} FITC labeled NP intake. Circles indicates internalized particles. For each condition two biological replicates (n = 2) with two technical replicates were included

FITC-C11 (Figure 4A, D), between 20 and 50 µg mL^{-1} FITC-P1C7 (Figure 4B,E) or between 20 and 50 µg mL^{-1} FITC-P1C5 samples (Figure 4C,F).

Also, based on confocal microscopy images, it was demanding to determine whether NPs are truly internalized or merely localized on cell membranes. For example, with FITC-P1C5 particles, clear clustering of the particles on the cell surface as well as potential internalization was observed (Figure 4C,F). In addition, with confocal microscopy great sample heterogeneity was observed between samples. As the MP-SPR results indicated the highest intake of C11 NP, additional confocal imaging was performed with these NPs. The confocal Z-stack images confirmed C11 NP intake and clear intracellular location as well (Figure 5) although FITC-labeling clearly decreased the cell intake as compared to label-free conditions when quantified with MP-SPR (Figure 3). As previously demonstrated and discussed with HeLa cells by Suutari et al. [23] it is reasonable to assume that the SPR responses do not originate merely as the result of NPs binding to the apical cell surface. Instead, the SPR responses indirectly reflect the cell uptake of NPs which consequently allows to detect the early endocytosis events providing supportive information to currently widely used label-based methods in NP.

The main aim of this study was to find out which NP formulation would be the most prominent for intake by hPSC-LSC and the timing of the maximal intake intensity. Based on the MP-SPR results, the label-free C11 resulted with highest signal. The P1C7 version of the NP was quite close with the signal level and the P1C5 NP had the lowest response. All NP formulations had the same relatively fast highest intake time point being around 20 minutes. It is known that the physicochemical properties of the NP can also greatly impact cellular intake and consequently in drug delivery efficacy.[19] Our results show that the smallest NP, C11, had the highest intake by hPSC-LSC, suggesting that the size of the NP is the most important feature regarding cellular intake by these therapeutic cells. Previous studies have also confirmed with other cell types that in general smaller NPs are easier to intake by cells than

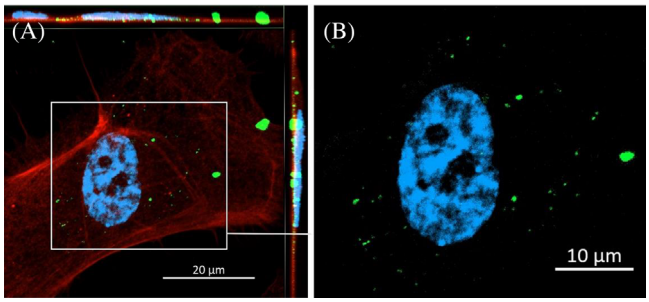

FIGURE 5 FITC labeled C11 intake by hPSC-LSC. (A) Confocal z-stack image confirms C11 intake by hPSC-LSC, already quantified with MP-SPR. FITC-labeled NPs (green), Hoechst (blue), and Phalloidin (red), scale bar is 20 µm. (B) C11 NPs localize near the cell nucleus of hPSC-LSC, scale bar is 10 µm. For the further confocal imaging two biological replicates (n = 2) with three technical replicates were included

26884011, 2022, 8, Downloaded from https://onlinelibrary.wiley.com/doi/10.1002/nano.202200027 by Tampere University Foundation, Wiley Online Library on [10/01/2023]. See the Terms and Conditions (https://onlinelibrary.wiley.com/terms-and-conditions) on Wiley Online Library for rules of use; OA articles are governed by the applicable Creative Commons License

larger NPs.[26,27] For the delivery of cargo, larger particle size of P1C5 would enable largest cargo yield (P1C5 surface area is 950 % larger than surface area of C11) but the final delivery yield is the fine balance of sufficient intake and the concentration of the cargo. Based on the MP-SPR data, the P1C7 signal responses are quite close to C11, if additional cargo delivery would be needed. However, it is also known that positively charged NPs are attracted to negatively charged cell membranes and are thus more prominent to cellular intake than non-charged or negatively charged NPs, since positive charge has the ability to disrupt the cellular bilayer.[26–28] Nevertheless, despite C11 has the highest internalization, it has the lowest zeta potential when compared to P1C5 and P1C7 in aqueous suspension. Moreover, the different chemical composition of the three formulations could lead to different protein corona formation as well as NP stability affecting thus cellular intake. Therefore, it was important to analyze the zeta potential of the NP formulations in cell culture medium used during intake studies (Figure S1 and Table S2). The difference in zeta potential values being slightly negative in the cell culture medium can be explained by the adsorption of proteins and other constituents of the cell culture medium on NPs surface.[29,30]

Strikingly, a clear difference between label-free and FITC-labeled light activatable polymeric NP was obtained in the intake signal by hPSC-LSCs. This is important result and highlights the need for label-free methods, like MP-SPR, for NP studies to obtain accurate intake results. The labeling affects the physico-chemical properties of NP. FITC dye is covalently conjugated to the primary amines of the NP, and therefore has impact in size, zeta potential, and hydrophobicity of the formulations. The FITC-labeled NP intake was further studied with confocal microscopy with both hPSC-LSCs and HeLa cells. Although, the confocal microscopy results did not fully correlate with MP-SPR results as with confocal microscopy the intake efficiency was low and concentration dependency or clear difference between the particle formulations could not be determined. However, lower intake of labeled NPs was uniformly observed from MP-SPR measurements for all three NP formulations and this phenomenon was probably seen also in confocal images. Much of the knowledge about internalization routes and NP properties has been determined by using fluorescent labeling of cells or NPs of interest. The drawback of using labeling agents is that the chemical modification introduced by the fluorescent probe can affect normal cell behavior or change the surface characteristics of the NPs. Thus, it would be beneficial to use of label-free methodologies capable of tracking NP cell intake in real-time to rule out possible interferences by labeling agents. Finally, the label-free MP-SPR based method enables increased reproducibility as well as concentration and time dependent intake analyses, providing tools to optimize the intake efficacy with lower NP concentrations and optimal administration timing for more sensitive cells including hPSC-LSCs.

3 | CONCLUSION

In this study, light activatable polymeric NP intake by living hPSC-LSCs was studied in real-time and label-free with MP-SPR technique. In addition, label-free and labeled NP intake was compared. The experimental set-up validation and sensor slide coating optimization was conducted first, followed by NP intake measurements of hPSC-LSCs with MP-SPR. Besides MP-SPR, confocal microscopy was utilized to validate FITC-labeled NP intake. The uniqueness of this study is to be the first MP-SPR intake study with hPSC-LSCs and light activatable polymeric NPs. MP-SPR is a novel tool to measure live cell NP intake in real-time and label-free. There are a few above mentioned publications reporting live cell NP intake with MP-SPR. However, these publications differ in their experimental setup, used cell types and NP formulations. Therefore, a straightforward comparison with previous studies cannot be conducted.

As a result, three different NP were studied with different concentrations and the NP C11, showed highest cellular intake. The C11 light activatable NP hold potential to be utilized in developing and studying NP-mediated modification method for hPSC-LSC-based therapies. Importantly, study demonstrated that the labeling of any of these three NPs has negative effect on cellular intake. These results highlight the need for the label-free methods to study cellular intake of NPs. For any therapy applications, validated non-invasive and label independent NP intake measurement systems implemented to the cell production would be important. The MP-SPR based approach presented in this study is foreseen to hold high potential in becoming a powerful platform for mechanistic studies of cell intake and cell interactions of various types of NPs. This is especially important with therapeutically relevant and highly sensitive hPSC-LSCs. The importance of tools cannot be over-expressed in the emerging field of nanomedicine for developing safe and efficient NPs for regenerative applications.

4 | EXPERIMENTAL SECTION

4.1 | Human PSC-LSC differentiation

All cell studies were conducted under the ethical approval of the Ethics Committee of Pirkanmaa Hospital District (Skottman/R05116) and no new cell lines were derived

26884011, 2022, 8, Downloaded from https://onlinelibrary.wiley.com/doi/10.1002/nano.202200027 by Tampere University Foundation, Wiley Online Library on [10/01/2023]. See the Terms and Conditions (https://onlinelibrary.wiley.com/terms-and-conditions) on Wiley Online Library for rules of use; OA articles are governed by the applicable Creative Commons License

from this study. The hPSC-LSCs were differentiated from the human embryonic stem cell lines Regea08/17 and maintained under serum- and feeder cell-free conditions as described previously.[25] For the experiments, cryopreserved hPSC-LSC in PSC cryopreservation medium (Thermo Fisher Scientific) were thawed at 37°C and directly plated on 4-well chamber slide (Nunc Lab-Tek II Chamber Slide System 4-well) or Nunc™ Thermanox™ plastic coverslips (Thermo Fischer), coated with 5 μg cm^{-2} CIV (Sigma-Aldrich) + 0.5 μg cm^{-2} L521 (Biolamina, Sundbyberg, Sweden). The cultures were maintained in defined CnT-30 corneal differentiation medium (CELLnTEC, Advanced Cell Systems) containing 0.5% antibiotics (P/S) at 37°C and 5% CO_2. Cell morphology and attachment were visually evaluated with a phase-contrast microscopy Zeiss Axio Vert A1 (Carl Zeiss). Intake studies with NPs were conducted when cells reached ~80% confluency and all main analyzes were conducted with two to three biological replicates in addition to method specific technical replicates.

4.2 | NP synthesis and characterization

The synthesis of the polymers C11, P1C5, and P1C7 and NP formation were prepared as mentioned in our earlier publications.[20,21] NP size was determined by DLS in a ZetaPALS analyser (Brookhaven Instruments Corp., Holtsville, NY). Zeta-potential was measured by using Zetasizer Nano Range (Malvern). Samples were defrosted from –80°C and labeled just before measurement. Sample concentration was 20 μg mL^{-1}. Zeta potential was measured after storing NPs 6 months in –80°C. Physicochemical properties of the NPs are described in Table S1 and Figure S1 and characterization of the zeta potential were also conducted in CnT-30 culture media used for cells during intake studies (Table S2). All NP samples can be stimulated with 365 nm ultraviolet light (UV-A) to release possible cargo. NPs were stored in –80°C and diluted in dH2O. NPs were defrosted only prior to use.

4.3 | NP labeling

C11, P1C7, and P1C5 NPs were labeled for MP-SPR measurements and confocal microscopy. First NP stock was taken from –80°C on ice. Once defrosted, 1 mg mL^{-1} NP stock was diluted to 0.1 mg mL^{-1} in 1x Borate Buffer pH 9.0 (Pierce™, Sigma-Aldrich), total sample volume being 1 mL. NP – Borate Buffer was vortexed (VWR Lab dancer) 2 seconds and sonicated 5 seconds (Eppendorf Centrifuge 5424 R). Then 1 μL of 1 mg mL^{-1} FITC (Sigma-Aldrich) diluted in dimethyl formamide (DMF) was added and mixed thoroughly. FITC binds to free amine groups on the NP surface. NP-FITC solution was incubated 2 hours at RT protected from light. Excess FITC was removed by centrifuging three times at 8000 × *g* for 8 minutes at +4°C. Both supernatant and resuspended NPs pellet were used to determine unbonded FITC and FITC covalently attached to NPs respectively, which was calculated by a calibration curve from known concentration of free FITC (0.01 to 1 μg mL^{-1}) prepared by diluting a stock solution of FITC in DMF with borate buffer, pH = 8.5 (linear regression equation y = 26557x (R^2 = 0.9937)).

4.4 | Quantification of NP intake

4.4.1 | NP feeding

For NP intake studies, FITC-labelled and unlabeled NPs were diluted in sterile milliQ-H20 in 1 mg mL^{-1}. NP suspension was then vortexed and sonicated with Bioruptor® sonicator (Diagenode Diagnostics) for 10 minutes. Before feeding to the cells, NPs were diluted into concentration 20 or 50 μg mL^{-1} in Cnt-30 cell culture medium and cells were incubated with NP suspension for 1 hour at +37°C the dark.

4.4.2 | hPSC-LSC immobilization on sensor slides

The hPSC-LSCs were plated with seeding density 40,000–50,000 cells cm^{-2}. After 24 hours incubation, hPSC-LSCs sensor slide was rinsed with warm PBS to remove unattached cells. Additionally, sensor slides were transferred to new wells to make sure there are no unattached cells growing on the glass side of the sensor. The hPSC-LSCs sensor slides, with different coatings, were imaged with light microscope after 72 hours incubation to validate which coating is the most optimal for hPSC-LSCs MP-SPR measurements.

4.4.3 | MP SPR measurements and data processing

MP-SPR measurements were carried out with MP-SPR NaviTM 200 OTSO (BioNavis, Tampere, Finland) instrument with two laser wavelengths (670 and 785 nm) measuring from each channel. The MP-SPR instrument was connected to an external peristaltic pump (Ismatec REGLO Digital MS-4/12) to ensure constant flow. Before each measurement, the fluidics were cleaned with 70% ethanol (Sigma-Aldrich), followed by a 10 min flow of 200 μL min^{-1}

26884011, 2022, 8, Downloaded from https://onlinelibrary.wiley.com/doi/10.1002/nano.202200027 by Tampere University Foundation, Wiley Online Library on [10/01/2023]. See the Terms and Conditions (https://onlinelibrary.wiley.com/terms-and-conditions) on Wiley Online Library for rules of use; OA articles are governed by the applicable Creative Commons License

dH2O. After cleaning, MP-SPR instrument fluidics was filled with Cnt-30 with 10 mM HEPES (Sigma-Aldrich) pH 7.4 with a flow rate of 200 μL min^{-1} for 10 minutes and temperature was set to +37°C. After that, cell sensor slides were inserted to the instrument and flow rate was set to 31 μL min^{-1} and cells were allowed to stabilize at least for 30 minutes.

C11, P1C7, and P1C5 NP were introduced for 14 minutes at 31 μL min^{-1} flow over the cell sensor slides in parallel to measurement channels. The post-wait time was 30 minutes after injection. Label-free 20 and 50 μg mL^{-1} C11, P1C7, and P1C5 (n = 3) intake by hPSC-LSCs was measured. FITC-labeled 50 μg mL^{-1} C11, P1C5, and P1C7 (for each concentration n = 1) intake by hPSC-LSCs was measured. Each cell sensor slide channel was used only once for NP sample injection. After measurement, sensor slides were stained with Trypan Blue (Gibco™) and imaged with Axio Vert A1 light microscopy to study cell viability.

MP-SPR measurement data was analyzed with BioNavis MP-SPR Navi™ Data Viewer (version 6.2.0) and sensogram graphs were created with TraceDrawer™ (version 1.8). Pre-injection time was set to 10 minutes, injection time was 14 minutes, and post-wait time was 30 minutes. Background signal was subtracted from the actual cellular response of up taking NPs. Additionally, the signal magnitude based on the exact number of live cells over the sensor slide was adjusted. These data analysis adjustments were done by subtracting 785 nm laser peak minimum signal from the 670 nm laser peak minimum signal from the same measurement channel. Though cells are cultured to 100% confluency over the sensor slide, the exact number of cells might not be the same between different sensor slides. This wavelength signal subtraction gives the absolute peak minimum change and represents the differential change of SPR. Therefore, the results of different measurements with the same experimental set-up can be compared to each other without knowing the exact cell number over sensor slide.

4.5 | In vitro cell analysis

After NP feeding, cells were fixed with 4% paraformaldehyde (PFA, Electron Microscopy Sciences, USA) for 20 minutes in RT, followed by 3x wash with DPBS. Cells were permeabilized with 0.1% Triton™ X-100 (Sigma-Aldrich) in DPBS for 15 minutes, followed by 3x wash with DPBS. To visualize filamentous actin cytoskeleton, cells were incubated with 1:800 phalloidin (Life Technologies Corporation) in 3% bovine serum albumin-PBS solution (3% BSA-PBS) for 30 minutes at RT. Excess phalloidin was removed by washing three times with DPBS for 5 minutes. To visualize cell nuclei, Hoechst trihydrochloride (Life Technologies Corporation) was added in final DPBS wash with 1:1000 v/v. Samples were mounted with ProLong® Gold antifade (Life Technologies Corporation).

4.6 | Confocal microscopy

Z-stack images from FITC-labeled C11, P1C7, and P1C5 intake by HeLa cells and hPSC-LSC were taken with Zeiss LSM 800 laser scanning confocal microscope (Zeiss, Jena, Germany) with a 63X/1.4 oil immersion objective. Nuclei were imaged with 465 nm laser (emission detected in blue), actin cytoskeleton with 568 nm (emission detected in red) and FITC labeled NPs with 488 nm (emission detected in green). Image processing was performed with Corel PHOTO-PAINT™ software (Corel corporation).

ACKNOWLEDGMENTS

The study was supported by grants from the Academy of Finland, Finnish Culture foundation, Instrumentarium foundation and Silmä- ja Kudospankki Foundation as well as financial support from POCI-01-0145-FEDER-029414 (acronym: LIghtBRARY) and UID/NEU/04539/2019 projects through Compete 2020 and FCT programs. MP-SPR instrument and reagents and guidance was provided by BioNavis Ltd. The authors acknowledge Teemu Suutari and Tapani Viitala for helping to transfer MP-SPR experimental set-up and giving guidance on the data analysis set-up. Outi Melin and Hanna Pekkanen are acknowledged for the production of hPSC-LSCs, Toni Montonen for the power density measurements and the Biocenter Finland and Tampere Imaging Facility (TIF) for the service.

REFERENCES

1. M. Griffith, D. G. Harkin, *Curr. Opin. Ophthalmol.* **2014**, *25*(3), 240. https://doi.org/10.1097/ICU.0000000000000049.
2. S. Ahmad, *Stem Cells Transl. Med.* **2012**, *1*(2), 110. https://doi.org/10.5966/SCTM.2011-0037.
3. C. Osei-Bempong, F. C. Figueiredo, M. Lako, *Bioessays* **2013**, *35*(3), 211. https://doi.org/10.1002/BIES.201200086.
4. M. Elsabahy, K. L. Wooley, *Chem. Soc. Rev.* **2012**, *41*(7), 2545. https://doi.org/10.1039/c2cs15327k.
5. S. Zhang, H. Gao, G. Bao, *ACS Nano*. **2015**, *9*(9), 8655. https://doi.org/10.1021/acsnano.5b03184.
6. S. Pinho, M. H. Macedo, C. Rebelo, B. Sarmento, L. Ferreira, *Drug Discovery Today* **2018**, *23*(5), 1071. https://doi.org/10.1016/j.drudis.2018.01.030.
7. M. M. Lino, L. Ferreira, *Drug Discovery Today* **2018**, *23*(5), 1062. https://doi.org/10.1016/j.drudis.2018.01.019.
8. X. Lin, X. Wu, X. Chen, B. Wang, W. Xu, *Int. J. Pharm.* **2021**, *602*, 120591. https://doi.org/10.1016/j.ijpharm.2021.120591.
9. T. Lajunen, R. Nurmi, L. Kontturi, L. Viitala, M. Yliperttula, L. Murtomäki, A. Urtti, *J. Control. Release* **2016**, *244*, 157. https://doi.org/10.1016/j.jconrel.2016.08.024.

26884011, 2022, 8, Downloaded from https://onlinelibrary.wiley.com/doi/10.1002/nano.202200027 by Tampere University Foundation, Wiley Online Library on [10/01/2023]. See the Terms and Conditions (https://onlinelibrary.wiley.com/terms-and-conditions) on Wiley Online Library for rules of use; OA articles are governed by the applicable Creative Commons License

10. G. Shim, S. Ko, D. Kim, Q. V. Le, G. T. Park, J. Lee, T. Kwon, H. G. Choi, Y. B. Kim, Y. K. Oh, *J. Control. Release* **2017**, *267*, 67. https://doi.org/10.1016/j.jconrel.2017.09.009.
11. L. A. Wells, S. Furukawa, H. Sheardown, *Biomacromolecules* **2011**, *12*(4), 923. https://doi.org/10.1021/bm101233m.
12. D. Vanhecke, L. Rodriguez-Lorenzo, M. J. D. Clift, F. Blank, A. Petri-Fink, B. Rothen-Rutishauser, *Nanomedicine* **2014**, *9*(12), 1885. https://doi.org/10.2217/NNM.14.108.
13. A. Elsaesser, A. Taylor, G. S. de Yanés, G. McKerr, E. M. Kim, E. O'Hare, C. V. Howard, *Nanomedicine* **2010**, *5*(9), 1447. https://doi.org/10.2217/nnm.10.118.
14. B. Drasler, D. Vanhecke, L. Rodriguez-Lorenzo, A. Petri-Fink, B. Rothen-Rutishauser, *Nanomedicine*, **2017**, *12*(10), 1095. https://doi.org/10.2217/nnm-2017-0071.
15. A. R. Collins *et al.*, *Wiley Interdiscip. Rev.: Nanomed. Nanobiotechnol.* **2017**, *9*(1). https://doi.org/10.1002/wnan.1413.
16. M. Vattulainen, T. Ilmarinen, T. Viheriälä, V. Jokinen, H. Skottman, *Stem Cell Res. Ther.* **2021**, *12*(1), 609. https://doi.org/10.1186/S13287-021-02673-3.
17. M. Vattulainen, T. Ilmarinen, L. Koivusalo, K. Viiri, H. Hongisto, H. Skottman, *Stem Cell Res. Ther.* **2019**, *10*(1), 236. https://doi.org/10.1186/s13287-019-1354-2.
18. R. Hayashi, Y. Ishikawa, T. Katayama, A. J. Quantock, K. Nishida, *Sci. Rep.* **2018**, *8*(1), 1. https://doi.org/10.1038/s41598-018-34845-2.
19. V. Francisco, C. Rebelo, A. F. Rodrigues, J. Blersch, H. Fernandes, L. Ferreira, *Methods* **2021**, *190*, 13. https://doi.org/10.1016/j.ymeth.2020.12.002.
20. J. Blersch, V. Francisco, C. Rebelo, A. Jiménez-Balsa, H. Antunes, S. Pinto, S. Simões, A. Rai, L. Ferreira, *Nanoscale* **2020**, *12*(18), 9935. https://doi.org/10.1039/c9nr10503d.
21. J. Blersch, V. Francisco, C. Rebelo, A. Jiménez-Balsa, H. Antunes, C. Gonzato, S. Pinto, S. Simões, K. Liedl, K. Haupt, L. Ferreira, *Angew. Chemie - Int. Ed.* **2020**, *59*(5), 1985. https://doi.org/10.1002/anie.201911398.
22. M. Notara, N. Refaian, G. Braun, P. Steven, F. Bock, C. Cursiefen, *Stem Cell Res.* **2015**, *15*(3), 643. https://doi.org/10.1016/J.SCR.2015.10.008.
23. T. Suutari, T. Silen, D. S En Karaman, H. Saari, D. Desai, E. Kerkelä, S. Laitinen, M. Hanzlikova, J. M. Rosenholm, M. Yliperttula, T. Viitala, *Small* **2016**, *12*(45), 6289. https://doi.org/10.1002/smLl.201601815.
24. M. A. Akl, A. Kartal-Hodzic, T. Suutari, T. Oksanen, I. M. Montagner, A. Rosato, H. R. Ismael, M. I. Afouna, P. Caliceti, M. Yliperttula, A. M. Samy, F. Mastrotto, S. Salmaso, T. Viitala, *ACS Omega* **2019**, *4*(16), 16878. https://doi.org/10.1021/acsomega.9b02086.
25. H. Hongisto, T. Ilmarinen, M. Vattulainen, A. Mikhailova, H. Skottman, *Stem Cell Res. Ther.* **2017**, *8*(1), 291. https://doi.org/10.1186/S13287-017-0738-4.
26. A. Panariti, G. Miserocchi, I. Rivolta, *Nanotechnol. Sci. Appl.* **2012**, *5*(1), 87. https://doi.org/10.2147/NSA.S25515.
27. N. Bertrand, J. Wu, X. Xu, N. Kamaly, O. C. Farokhzad, *Adv. Drug Deliv. Rev.* **2014**, *66*, 2. https://doi.org/10.1016/j.addr.2013.11.009.
28. B. Yameen, W. Il Choi, C. Vilos, A. Swami, J. Shi, O. C. Farokhzad, *J. Control. Release* **2014**, *190*, 485. https://doi.org/10.1016/j.jconrel.2014.06.038.
29. K. Strojan, A. Leonardi, V. B. Bregar, I. Križaj, J. Svete, M. Pavlin, *PLoS One* **2017**, *12*(1), e0169552. https://doi.org/10.1371/JOURNAL.PONE.0169552.
30. L. Estronca, V. Francisco, P. Pitrez, I. Honório, L. Carvalho, H. Vazão, J. Blersch, A. Rai, X. Nissan, U. Simon, M. Grãos, L. Saúde, L. Ferreira, *Nanoscale Horiz.* **2021**, *6*(3), 245. https://doi.org/10.1039/D0NH00550A.

SUPPORTING INFORMATION

Additional supporting information may be found in the online version of the article at the publisher's website.

How to cite this article: M. Kauppila, R. Ståhlberg, V. Francisco, L. Ferreira, H., Skottman. *Nano Select*. **2022**, *3*, 1232. https://doi.org/10.1002/nano.202200027

26884011, 2022, 8, Downloaded from https://onlinelibrary.wiley.com/doi/10.1002/nano.202200027 by Tampere University Foundation, Wiley Online Library on [10/01/2023]. See the Terms and Conditions (https://onlinelibrary.wiley.com/terms-and-conditions) on Wiley Online Library for rules of use; OA articles are governed by the applicable Creative Commons License